

# A Molecular Model of the Human UDP-Glucuronosyltransferase 1A1, Its Membrane Orientation, and the Interactions between Different Parts of the Enzyme<sup>[S]</sup>

Liisa Laakkonen and Moshe Finel

*Centre for Drug Research, Faculty of Pharmacy, University of Helsinki, Helsinki, Finland*

Received December 22, 2009; accepted March 9, 2010

## ABSTRACT

The vertebrate UDP-glucuronosyltransferases (UGTs) are membrane-bound enzymes of the endoplasmic reticulum that process both endogenous and exogenous substrates. The human UGTs are well known biologically, but biophysical understanding is scarce, largely because of problems in purification. The one resolved crystal structure covers the C-terminal domain of the human UGT2B7. Here, we present a homology model of the complete monomeric human UGT1A1, the enzyme that catalyzes bilirubin glucuronidation. The enzyme can be seen as composed of four different domains: two large ones, the N- and C-terminal domains, and two small ones, the “envelope” helices and the transmembrane segment that includes the cytoplasmic tail. The hydrophobic core of the N-terminal domain and the two envelope helices that connect the large domains

are shown to be structurally well conserved even among distant homologs and can thus be modeled with good certainty according to plant and bacterial structures. We consider alternative solutions for the highly variable N-terminal regions that probably contribute to substrate binding. The bilirubin binding site, known pathological mutations in UGT1A1, and other specific residues have been examined in the context of the model with regard to available experimental data. A putative orientation of the protein relative to the membrane has been derived from the location of predicted N-glycosylation sites. The model presents extensive interactions between the N- and C-terminal domains, the two envelope helices, and the membrane. Together, these interactions could allow for a concerted large-scale conformational change during catalysis.

UDP-glycosyltransferases catalyze the transfer of sugar groups, activated by uridine diphosphate (UDP-sugar), to small-molecule acceptor substrates. The most commonly used sugar is glucose, and the range of acceptor substrates is seemingly infinite. Glycosyltransferases are found in all kingdoms of life and are involved in biosynthesis, biotransformations, signal transduction, and metabolism. Despite this tremendous functional variability, all structurally known glycosyltransferases that use sugar nucleotides as donors adopt one of only two different folds, GT-A or GT-B, and are readily identified by a 44-residue-long “signature sequence” at the UDP-sugar binding site (Prosite pattern PS00375; <http://au.expasy.org/prosite>). Both GT-A and GT-B folds comprise two  $\alpha/\beta/\alpha$  sandwich domains that, in the GT-A fold, are packed closely together to form a continuous central

$\beta$ -sheet. In the GT-B fold enzymes, including the human UDP-glucuronosyltransferases (UGTs), the two domains are connected by a flexible linker (Unligil and Rini, 2000; Lairson et al., 2008). The contrast between multiple biological roles and very similar structures highlights the functional importance of local structural differences.

The vertebrate UGTs transfer the glucuronic acid moiety from UDP-GlcUA to lipophilic acceptor substrates in an  $S_N2$  reaction. The reaction proceeds stepwise: UDP-GlcUA binds first to the enzyme and primes it for the binding of the acceptor substrate. After the sugar transfer, the ternary complex resolves and the product dissociates from the enzyme. Substrate inhibition is often observed, and it has been interpreted as formation of a nonproductive enzyme–UDP–substrate complex (Luukkanen et al., 2005).

A single C-terminal transmembrane helix anchors the UGTs to the endoplasmic reticulum membrane, whereas most of their mass is on the luminal side. Secondary membrane attachment sites have been proposed (Ciotti et al., 1998; Ouzzine et al., 1999). The cellular localization and membrane attachment separate the vertebrate UGTs from

This work was supported by the Sigrid Juselius Foundation and the Magnus Ehrnrooth Foundation.

Article, publication date, and citation information can be found at <http://molpharm.aspetjournals.org>.  
doi:10.1124/mol.109.063289.

[S] The online version of this article (available at <http://molpharm.aspetjournals.org>) contains supplemental material.

**ABBREVIATIONS:** UGT, UDP-glucuronosyltransferase; GT, glycosyltransferase; PDB, Protein Data Bank; CN-I, Crigler-Najjar type I; CN-II, Crigler-Najjar type II.

the bacterial and plant glycosyltransferases, which are mostly water-soluble proteins in the cytoplasm. The transmembrane helix of the vertebrate UGTs is important for activity (Meech et al., 1996; Kurkela et al., 2004a,b), and UGTs probably exist as oligomers (Finel and Kurkela, 2008), but the physical details of these features are currently unknown.

The crystal structure of the C-terminal domain of the human UGT2B7 has been resolved (Miley et al., 2007) and agrees well with other known GT-B structures. In complete GT-B structures (see Fig. 1), the two major domains are connected by a central extended linker of approximately 10 residues and two C-terminal “envelope” helices, each approximately 20 residues long, that fold back over both domains (e.g., Brazier-Hicks et al., 2007).

The human UGTs have different, but partly overlapping, substrate specificities. By sequence similarity and gene structure, the human UGTs can be clustered into two groups, UGT1A and UGT2 (Mackenzie et al., 2005). The glucuronidation of bilirubin, the neurotoxic breakdown product of heme, is catalyzed by UGT1A1 and is essential for its biliary excretion (Bosma et al., 1994). Mutations that lower UGT1A1 expression level or reduce its activity result in elevated levels of free bilirubin in the serum, leading to Crigler-Najjar type I (CN-I) or II (CN-II) syndrome or Gilbert syndrome.

Six homology models have been published of two-domain UGTs: two of the human UGT1A1 (Li and Wu, 2007; Locuson and Tracy, 2007), one of the human UGT1A9 (Fujiwara et al., 2009a), and three of the plant enzymes UGT73A5 (Hans et al., 2004), UGT85B1 (Thorsøe et al., 2005), and UGT94B1

(Osmani et al., 2008). The two UGT1A1 models and the UGT94B1 model are built on the same template UGT71G1 of *Medicago truncatula* (PDB ID code 2acv), the UGT1A9 model is based on the structure of GtfA from *Amycolatopsis orientalis* (PDB ID code 1pn3), and the slightly older UGT73A5 and UGT85B1 models use GtfB of *A. orientalis* as the template (PDB ID code 1iir). All of these models lack some parts of the enzyme: the envelope helices or some central loops in the N-terminal domain.

We have constructed an all-atom model of the monomeric human UGT1A1. The model highlights extensive interactions between different parts of the enzyme, proposes an orientation with respect to the membrane, and suggests molecular explanations for pathological mutations.

## Materials and Methods

The UGT1A1 sequence P22309 from the SwissProt database (<http://www.uniprot.org>) was used in this study. Protein structures related to the human UGT1A1 sequence were searched by both sequence and structure comparisons, using the program PSI-BLAST (Altschul et al., 1997) against the Protein Data Bank (Berman et al., 2000) and the program Dali (Holm et al., 2008). Structurally annotated sequence alignments were rendered with Alscript (Barton et al., 1993). Once identified, 13 structural relatives of UGT1A1 were superimposed with a tcl script (<http://www.tcl.tk>) in the program VMD (Humphrey et al., 1996). For the N-terminal domain, the atoms selected for superposition were 66 C $\alpha$ s from the seven  $\beta$ -strands and helices N $\alpha$ 1 and N $\alpha$ 4 (see Supplemental Fig. 1); and for the C-terminal domain, 73 C $\alpha$  atoms were selected from the  $\beta$ -strands and helices C $\alpha$ 3, C $\alpha$ 4, and C $\alpha$ 5. Secondary structure was predicted for

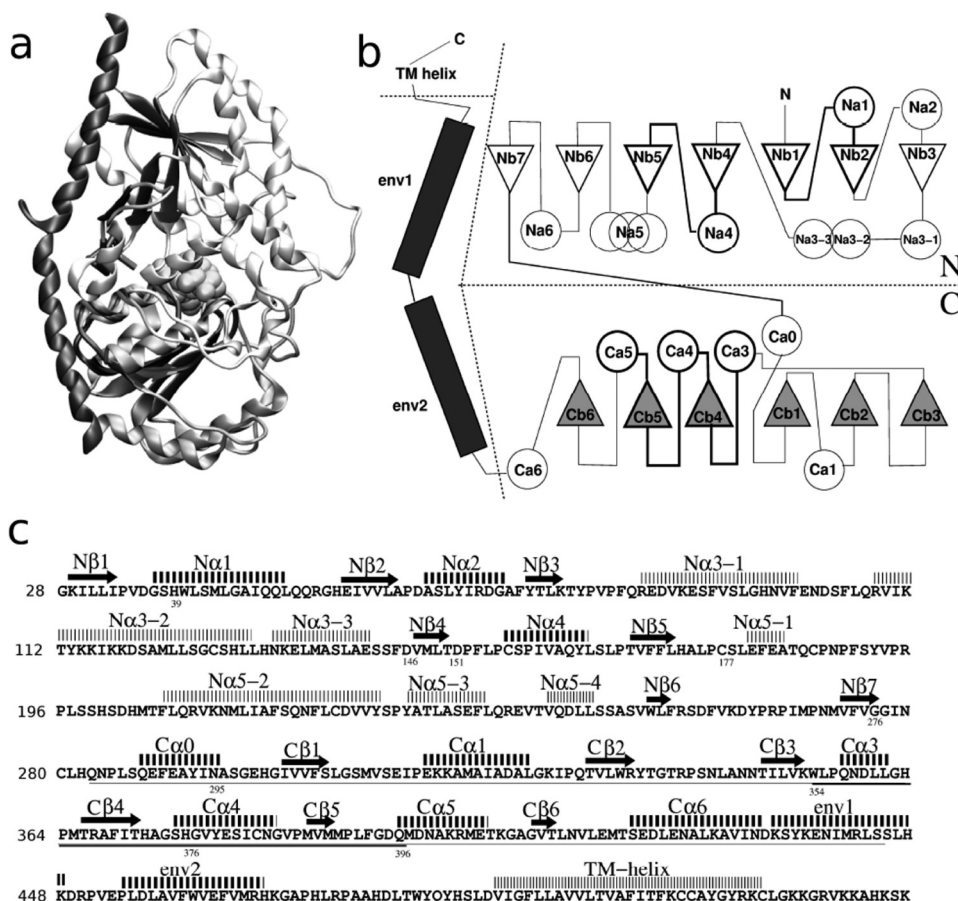


**Fig. 1.** Structure of the UGT1A1. a, one of the GT-B fold templates, UGT72B1 from *Arabidopsis thaliana* (PDB ID code 2vce; Brazier-Hicks et al., 2007). Helices are shown as spirals, and  $\beta$ -strands are shown as arrows. The N-terminal domain is on the top, the C-terminal domain is on the bottom, and the envelope helices are on the left. The core  $\beta$ -strands are shaded dark. The space-filling molecule between the domains is the UDP-sugar bound in the active site. The molecular images were rendered with VMD (Humphrey et al., 1996). b, predicted topology diagram for UGT1A1.  $\beta$ -Strands are represented by triangles, core helices by spheres, and envelope helices by rectangles. Well conserved structural elements are drawn as thick lines. Helices in loop 5 are not shown individually. The N and C termini are marked with N and C, respectively, and the four structural domains are separated by dashed lines. The image was drawn with Xfig (<http://www.xfig.org>). c, the position of the secondary structure elements in the UGT1A1 sequence, based on the structural alignment of known GT-B structures and all human UGT sequences. Strands are marked with arrows, and helices are indicated by dashed lines.

the target sequence with the program PredictProtein (Rost et al., 2004). The same prediction program was run for four selected templates as a test, and the results agreed well with the known structures (data not shown).

The secondary structure elements were named by the domain, N or C;  $\beta$ -strands in each domain core were numbered ( $\beta 1$ – $\beta 7$ ), and helices were given the number of the strand they follow, supplemented by a sequential subnumber when needed. For example, N $\alpha 1$  stands for the  $\alpha$ -helix in the N-terminal domain that follows strand  $\beta 1$  of this domain, and N $\alpha 3$ -1 stands for the first segment in the  $\alpha$ -helix that follows strand  $\beta 3$  of the N-terminal domain. The pre-strand helix in the C domain was called C $\alpha 0$ . The nomenclature resembles those used by others (Unligil and Rini, 2000; Li and Wu, 2007; Miley et al., 2007). Amino acid numbers refer to the full-length human UGT1A1, unless mentioned otherwise.

The 19 human UGT sequences were aligned to each other by using ClustalX 2.0.5 (Larkin et al., 2007). The UGT alignment was matched to the structural alignment of the selected GT-B proteins, including the predicted secondary structure elements as weight factors. Two alignments were constructed for N $\beta 4$ , aligning either Asp146 or Asp151 as the aspartate situated right behind the catalytic histidine of the known structures. For residues 83 to 143, three sequence-to-structure matches were considered. The rotational orientation of helix N $\alpha 3$ -2 relative to the rest of the protein is the same in each of them, but the position of the sequences relative to the structures differs by one helical turn. The envelope helices were modeled at residues 434 to 448 and 454 to 467 according to the templates, and the transmembrane helix was constructed as a standard  $\alpha$ -helix at residues 491 to 516.

Homology models were constructed by using the program Modeller 9v6 with a standard modeling scheme, very thorough annealing, and molecular dynamics optimization (Sali and Blundell, 1993). Three templates were used for the N-terminal domain (PDB ID codes 2vce, 1iir, and 2iya) and one for the C-terminal domain (PDB ID code 2o6l). The nonhydrolyzable UDP-glucose analog (residue name UF2) was copied from the 2vce structure and included in the model as a block residue. Likewise, an N-linked branched sugar [N-acetyl-D-glucosamine)-(N-acetyl-D-glucosamine)-(β-mannose-(α-mannose)-(β-mannose)], was copied from 3d12 and attached to the residues predicted to be glycosylated by NetNGlyc (<http://www.cbs.dtu.dk/services/NetNGlyc>; R. Gupta, E. Jung, and S. Brunak, manuscript in preparation). The residues corresponding to the predicted UGT-glycosylation sites were changed to asparagines in structure 1iir (Ala44 and Asp235) to allow for the binding of the N-glycosylamine. Helical conformation was constrained between residues Val491 and Lys516 for the predicted transmembrane helix (Rost et al., 2004). Fifty structures were modeled and optimized. The majority of these jobs finished successfully, and the 10 with the best values of the target function were studied in detail. The stereochemical quality of the models is good, as analyzed by MolProbity (data not shown) (Davis et al., 2007), whereas optimization violations occur in the long loops, as expected. The model coordinates are available on request (liisa.laakkonen@helsinki.fi).

A molecular structure for (Z,Z)-bilirubin was retrieved from the PubChem database (<http://pubchem.ncbi.nlm.nih.gov>). It was modified to correspond to the experimentally resolved ridge-tile configurations E,E and E,Z (Nogales and Lightner, 1995) and optimized in MOPAC2009 (<http://openmopac.net>) with PM3 methodology (Stewart, 2007). The substrate structures were docked manually to the final enzyme model between the active-site histidine, His39, and the nonhydrolyzable UDP-glucose analog.

A list of nonsynonymous CN-I mutations was gathered from the UGT allele site (<http://www.pharmacogenomics.pha.ulaval.ca>), and the mutations were localized into the protein model.

The new UGT1A1 model was compared with previous ones done by Locuson and Tracy (2007) and Li and Wu (2007). The basis for the comparison was a structural alignment between UGT71G1 from *M.*

*truncatula* (PDB ID code 2acv) and GtfD from *A. orientalis* (PDB ID code 1rrv), onto which the UGT1A1 sequences were added manually as described in the previous studies. A direct structural comparison could not be performed because the coordinates of the earlier models were not available.

## Results

**Structurally Related Proteins.** We divided the human UGT into four different substructures: the N-terminal domain, the C-terminal domain, the envelope helices, and the transmembrane segment (Fig. 1). For the C-terminal domain and the envelope helices there are good structural templates, and the single transmembrane helix can be safely modeled de novo, but the N-terminal domain requires special attention. It has no high-homology templates; therefore, we first analyzed the available low-homology templates to identify structurally conserved features that could guide the construction. To avoid biasing the modeling toward either plant or bacterial templates, several representative templates were used for the modeling.

Structural relatives of UGT1A1 were searched by both sequence and structure comparisons. The sequence similarity search with PSI-BLAST against the Protein Data Bank converged in five rounds onto 15 hits with expectation values below  $10^{-30}$ . The expectation values of the next best proteins were  $>1$ . The hit structures also were found to be true homologs by visual evaluation. It is noteworthy that all local similarities between the query and hit sequences correspond to the respective C-terminal domains.

The structural similarity search on Dali could not be done with UGT1A1, but the partial structure of UGT2B7 was used as a query. Nevertheless, the outcome of the Dali search overlapped with the PSI-BLAST results, as expected. The separation of glycosyltransferases from the next group of enzymes, glycosyl epimerases, was not as clear-cut in Dali as in the sequence search. Dali returns both chains of crystallographic dimers as independent hits. In such cases only the first of the two monomers was recorded. Another issue we had to address was sequence redundancy among the search results. By sequences, structures 2acv and 2acw are 100% identical as are the 2vg8 (or 2vcu)/2vce/2vch, 2c1x/2c9z/2c1z, and 3d0q/3d0r groups. Only one structure of each set was considered in the structural alignment.

Finally, 13 unique structures were considered representative of the GT-B fold and potentially good templates for modeling the human UGT1A1 (Table 1). The 13 proteins were superimposed for structural analysis (see Supplemental Fig. 1 for structural alignment and original references). Overlaying complete proteins by core  $\beta$ -strands did not give good results, because the interdomain angles vary between structures, but aligning either the N- or C-terminal domains separately yielded good matches. The pairwise root-mean-square deviation values between the templates for 66 C $\alpha$  atoms in the N-terminal domains ranged from 0.58 to 2.24 Å, with a mean of 1.42 Å. The corresponding values for 73 C $\alpha$  atoms in the C-terminal domains were 0.51, 1.81, and 1.25 Å. The same sets of atoms were used for all pairwise comparisons.

The GT-B structures cluster by their biological roles, sequence identities, and root-mean-square deviations into four mutually similar groups: 1) human UGT2B7 (PDB ID code



2o6l), 2) plant UGT enzymes (PDB ID codes 2vce, 2acv, 2c1x, and 2pq6), 3) bacterial glycosyltransferases (PDB ID codes 1iir, 1rrv, 1pn3, 1f0k, and 2p6p), and 4) macrolide glycosyltransferases from *Streptomyces* (PDB ID codes 2iya, 2iyf, and 3d0q). Three structures were selected to serve as a template for modeling the N-terminal domain of UGT1A1, one each from groups 2 to 4 (PDB ID codes 2vce, 1iir, and 2iya), and the 2O6L structure was the template for the C-terminal domain. In addition, helix Nα3-1 was constructed according to structure 2p6p of group 2.

**Analysis of the Template Structures.** The template proteins fold into canonical GT-B structures of two α/β/α domains with parallel β-strands. Strands and helices alternate throughout the structure, with a few exceptions (see Fig. 1). Both the N- and C-terminal β-sheets follow similar topology, 3-2-1-4-5-6(-7), but they differ in that the former are strongly twisted, whereas the latter are rather flat. The angles between the strands at opposite edges are approximately 110 and 40° in the N- and C-terminal domains, respectively. Despite the similar folds, the two-domain structures vary in length by more than 70 amino acids among the 13 templates. One reason is that in the shorter bacterial enzymes the last helix in the N-terminal domain, Nα6, is replaced by a coil. Major length variations are also found in the segment between Nβ5 and Nβ6.

The core β-strands are structurally well conserved in both domains, but the best-conserved helices occur asymmetrically. In the N-terminal domains, the conserved helices are Nα1 and Nα4 that embrace strands Nβ1, Nβ2, Nβ4, and Nβ5 at the center of the twisted sheet. In the C-terminal domains the best-conserved helices are Cα3, Cα4, and Cα5, lying above the flat β-sheet and facing the active site at the center of the protein (see Fig. 1b). These helices were used in the structural superpositions in addition to the core β-strands.

Eight of the studied GT-B protein structures are complete, whereas the other five end at various positions within the envelope helices. The two envelope helices are connected by a short linker that adopts different conformations in the structures. In addition to variations of the angle between the N- and C-terminal domains, the structures exhibit pronounced variation at two other sites: between strands Nβ3 and Nβ4 and between strands Nβ5 and Nβ6. Instead of folding into single helices such as most interstrand segments, these two

long stretches contain several ordered helices. Here, we call the complete segments loops 3 and 5 and number the included helices sequentially (Fig. 1).

Loop 3 is 42 to 57 residues long. After Nβ3 the polypeptide chain first continues along the direction of that strand, either as a random coil or a helix, but 10 to 15 residues later the chain turns and folds back as a helical structure. The early part of loop 3 is disordered in many crystal structures, implying mobility, but the shared helices are well resolved and pack to their surroundings. The first helix interacts with a helix in loop 5, whereas the second packs to Nα4. The overall path of loop 3 helices is similar in all template proteins, even though the helical feature is straight and continuous in the bacterial proteins, but is kinked in the plant proteins. The end halves overlap well structurally, but because of different helix geometries, the starting points differ by approximately 12 Å between the plant and bacterial proteins. The helices are clearly amphipathic: their hydrophobic faces pack to the protein core, and the hydrophilic faces toward the neighboring helices and the solvent. It is noteworthy that there are many specific interactions between residues in Nα3 and its surroundings in the known proteins. For example, the following pairs are observed: structure 2vce, Ser87/Asn200, Thr91/Asp122, Arg92/Asp75, and Arg98/Glu129; structure 1iir, Thr76/Arg165 and Phe84/His173; and structure 2p6p, Arg86/Glu71, Arg90/Glu7, and Arg98/Asp55.

Loop 5 between strands Cβ5 and Cβ6 is highly variable; its scatter in length, from 37 to 85 residues, and structural features are larger than any other part of the studied GT-B proteins. It folds into a compact shape and, like loop 3, is discontinuous in several crystal structures. The 10 residues closest to the flanking β-strands follow similar paths in the plant and bacterial proteins, whereas the rest of the peptide chain adopts totally different structures in these two groups. In the plant enzymes, the loop starts and ends with 10-residue helices, between which there are tiny helices and strands. The mass of the loop is oriented toward the C-terminal domain of the enzyme. In the bacterial proteins, the body of the loop reaches to the N-terminal domain, and its main structural feature is a long bent helix in the latter part of the loop that packs to the latter half of helices Nα3 and Nα4. The length of the loop before this helix varies from five to 25 amino acids and reveals no shared characteristics.

TABLE 1  
Structural relatives of the human UGT1A1

Only unique sequence hits are shown. For the PSI-Blast search, the expectation value is given, and for the Dali searches the z-score is given. Structure 2o6l was used as the query in the Dali search. Sources are given of modeling work where a structure has been used as a template.

PDB ID Code	Source Species	Source	PSI-Blast	Dali	Used as a Template (Source)
2acv	<i>Medicago truncatula</i>	Triterpene UGT71G	10 <sup>-51</sup>	21.2	Li and Wu, 2007; Locuson and Tracy, 2007; Osmani et al., 2008
2c1x	<i>Vitis vinifera</i>	UDP-glucose flavonoid GT	2 × 10 <sup>-50</sup>	20.7	
1iir	<i>Amycolatopsis orientalis</i>	GtfB	5 × 10 <sup>-50</sup>	19.3	Hans et al., 2004; Thorsøe et al., 2005; current study
2pq6	<i>Medicago truncatula</i>	Multifunctional GT	7 × 10 <sup>-46</sup>	21.3	
2iya	<i>Streptomyces antibioticus</i>	Macrolide GT	2 × 10 <sup>-45</sup>	21.3	Current study
2iyf	<i>Streptomyces antibioticus</i>	Macrolide GT	6 × 10 <sup>-45</sup>	20.3	
1rrv	<i>Amycolatopsis orientalis</i>	GtfD	10 <sup>-44</sup>	19.6	Locuson and Tracy, 2007
2o6l	<i>Homo sapiens</i>	UGT2B7	10 <sup>-44</sup>	36.1	Current study
1pn3	<i>Amycolatopsis orientalis</i>	GtfA	2 × 10 <sup>-39</sup>	18.5	Thorsøe et al., 2005; Fujiwara et al., 2009a
2vce	<i>Arabidopsis thaliana</i>	UGT72B1	10 <sup>-42</sup>	20.3	Osmani et al., 2008; current study
2p6p	<i>Streptomyces fradiae</i>	C-C bond forming GT	2 × 10 <sup>-39</sup>	16.8	Current study for Nα3-1
3d0q	<i>Micromonospora echinospora</i>	CALG3	9 × 10 <sup>-39</sup>	17.8	
1f0k	<i>Escherichia coli</i>	MurG	4 × 10 <sup>-36</sup>	14.1	

**UGTs: from Sequences to Structures.** The sequence identities of the mature proteins are approximately 70% within the UGT1As, 75% among the UGT2s, and 45% between the two groups. The corresponding values for the N-terminal domains are 40, 50, and 30%. Aligning the mature UGT sequences is simple because of their high mutual similarity. Their lengths vary by merely two residues, 504 to 506, and gaps are required in the multiple alignment at only seven sites: after residues 77, 97, 102, 175, 226, 508, and 516 (Supplemental Fig. 1). The four latter sites are single gaps. Of the 504 to 506 residues, 145 are identical in all human UGTs. Against this overall similarity, the sequence variation around residues 77, 97 to 102, and 175 is striking, and the local sequence alignment becomes ambiguous.

Matching the 19 human UGT sequences to the 13 GT-B structures is trivial for the C-terminal domain because UGT2B7 is included in both the structural and the sequence alignment. The residues in the “signature sequence” form a central part of the C-terminal domain, covering C $\alpha$ 3, C $\beta$ 4, C $\alpha$ 4, and C $\beta$ 5. As has been discussed earlier (Miley et al., 2007), residues involved in binding the shared sugar donor are found conserved in this segment (Trp354, Gln357, His372, Glu380, Phe394, Asp396, and Gln396). The additional conserved residues in the segment (Leu360, Leu361, Phe369, Ile370, Thr371, Ser381, Ile382, and Met388) form the tightly packed hydrophobic core of the C domain.

All  $\beta$ -strands, and helices N $\alpha$ 1 and N $\alpha$ 4 and the two envelope helices, align well to the template structures (see Fig. 1 and Supplemental Fig. 1). On the contrary, the variable loops 3 and 5 could be aligned in several different ways. Sequence homology is insufficient for smooth modeling without additional input. We have included secondary structure predictions, physical considerations derived from the templates, and biological data on the UGTs in the modeling. The area of N $\beta$ 4 was studied in detail because of recent conflicting data (Li et al., 2007; Patana et al., 2008). In this area, the most striking feature of the GT-B structural alignment is a fully conserved stretch of hydrophobic amino acids at the center of N $\beta$ 4, with aspartates at both ends. Neither of the acids is fully conserved among the 13 template proteins, and neither one lacks matching acidic residues. In our preferred sequence-to-structure alignment (Supplemental Fig. 1), the two UGT aspartates are located at the beginning and end of N $\beta$ 4, 16 Å apart from each other. This places Asp151 next to the active site, in hydrogen-bonding distance from His39, whereas Asp146 is located at the beginning of strand N $\beta$ 4. In the GT-B proteins studied, aspartates at the proposed position for Asp146 of UGT1A1 form hydrogen bonds to the beginning of N $\beta$ 1 and the end of the second envelope helix. In line with this, Asp146 in the model comes into contact with Lys29 and Lys469. In the alternative alignment the sequence is moved forward by five residues, bringing Asp146 next to the catalytic histidine. The second aspartate, Asp151, is now situated in the loop between N $\beta$ 4 and N $\alpha$ 4, where it can interact with the substrates. This change is feasible because loop 3 is of sufficient length and low homology, but it leads to an alignment in which the center of N $\beta$ 4 is no longer universally hydrophobic, and the fork position before N $\beta$ 4 is occupied by Ala141 (data not shown). In addition, the size of the substrate binding cavity is reduced.

Loop 3 of UGT1A1, with its 65 residues, is longer than the same loop in any of the templates (42–57 amino acids). It is

predicted to contain three helices, N $\alpha$ 3-1 (Arg85/Val99), N $\alpha$ 3-2 (Phe105/Leu130), and N $\alpha$ 3-3 (Lys134/Ala141). Most probably, two of these correspond to the helical stretch seen in all the templates. If N $\alpha$ 3-1 and N $\alpha$ 3-2 correspond to the shared helices, the extra helix will fold at the far end of the protein, close to the N terminus. And, if N $\alpha$ 3-2 and N $\alpha$ 3-3 make for the shared feature, N $\alpha$ 3-1 will lie at the interface between the large domains. We find the latter alternative more likely. First, the templates show structural variability before the long helical stretch, but none after it. Second, many residues in loop 3 affect activity in various UGTs and supposedly contribute to the binding site at the domain interface (Lewis et al., 2007; Nishiyama et al., 2008; Fujiwara et al., 2009a,b). Accordingly, the predicted helices N $\alpha$ 3-2 and N $\alpha$ 3-3 of UGT1A1 are matched to the two shared loop 3 helices of the templates (Supplemental Fig. 1). The additional helix, N $\alpha$ 3-1, is built at the domain interface according to an analogous extra helix in structure 2p6p.

The resulting helical segment N $\alpha$ 3-2/3 is longer than what is observed in the templates (37 versus 23–30 amino acids) and reveals no obvious sequence-to-structure match. The single conserved property of N $\alpha$ 3s in the studied GT-B proteins is amphiphilicity and, indeed, a periodic separation of hydrophobic and hydrophobic residues is also visible in the UGT alignment. This dictates the rotational orientation of the sequences to the structure. The gap in the N $\alpha$ 3-2/3 helix predictions (residues 131 and 132) would naturally match the interhelical kink of many templates, in which case N<sub>133</sub>K<sub>134</sub>E<sub>135</sub> of UGT1A1 would align to N<sub>89</sub>P<sub>90</sub>E<sub>91</sub> of structure 2vce. However, lacking any clear sequence similarity between human UGTs and the template proteins in this region, three different alignments were constructed, varying the position by one helical turn at a time. The first match is as suggested above, the next matches NPE of structure 2vce to the L<sub>130</sub>L<sub>131</sub>H<sub>132</sub> of UGT1A1, and the third to C<sub>127</sub>S<sub>128</sub>H<sub>129</sub> of the human enzyme. The resulting model options are called c, b, and a, respectively. All three models yield stable structures of comparable energies. There are large structural variations in loop 3 between individual model structures, however, reflecting the poor homology of UGTs to any template and conflicting template structures. Again, several polar interactions are observed between residues in loop 3 and its surroundings.

The other highly variable segment, loop 5, is 77 residues long in UGT1A1, well within the observed length variation in the template structures. Sequence analysis strongly predicts one long helix from Phe206 to Val226, followed by two shorter ones at 230 to 237 and 244 to 248 (Fig. 1b). This pattern of three helices close to N $\beta$ 6 agrees with the structures of the bacterial proteins, but not the plant proteins. Hence, structure 1iir was chosen as the sole template for modeling loop 5. Some sequence similarity can be observed between the UGTs and the bacterial templates at the end of this segment. An additional, weakly predicted helix was built de novo for the early part of the loop, at Leu179 to Glu182.

Figure 2 shows a superposition of the 10 lowest-energy model structures. They are practically indistinguishable from each other at the C-terminal domain, where a good template was available. It is noteworthy that the structures match reasonably well also for the core of the N-terminal domain and the envelope helices. Reflecting both the struc-

tural and sequence analyses, the path of the peptide chains vary remarkably in loops 3 and 5, while always folding back to a compact structure. No nonphysical strongly extended loops out of the protein core were observed.

**Nonhomology Modeling.** To get a complete view of the functional protein, even if some parts are more hypothetical, we also modeled the transmembrane segment and the N-linked complex sugars. They were constructed by combining sequence data to molecular knowledge on other proteins. In general, transmembrane helices show well characterized properties, especially in single-pass proteins (White, 2009). The predicted transmembrane segment of UGT1A1 was built as a standard  $\alpha$ -helix from Val491 to Lys516, as predicted. This is longer than the 17 hydrophobic residues, Val491 to Phe507, that are often taken as the membrane-intercalated segment of the UGTs. Without additional data on intramolecular interactions, the orientation of the helix with respect to the globular part was left undetermined.

The orientation of UGT1A1 relative to the membrane was addressed from another, unrelated point of view: the N-linked glycosylation sites. The very hydrophilic and mobile branched sugar groups cannot exist but in an aqueous environment. The high sequence similarity among the human UGTs strongly suggests that they all fold very similarly and, therefore, are oriented to the membrane in the same way. Accordingly, we have analyzed the glycosylation sites in all human UGTs and located these sites on the structural model of UGT1A1. The likelihood of the NXS/T sequence motifs to be glycosylated was predicted by NetNGlyc (<http://www.cbs.dtu.dk/services/NetNGlyc>), and the results are shown in Fig. 3. Only one glycosylation site was predicted for UGT1A1, Asn295 in  $C\alpha 0$ , that is shared by all UGT1A enzymes. In the model, Asn295 points out of the protein and could easily accommodate a large and mobile sugar unit. The UGT2 enzymes lack the glycosylation site at  $C\alpha 0$ , but there is an alternative site eight residues later, corresponding to Glu303 in UGT1A1. It lies before the start of  $C\alpha 1$ , close to the domain interface.

In all other human UGTs, with the exception of UGT1A1 and UGT2B4, at least one glycosylation site is predicted

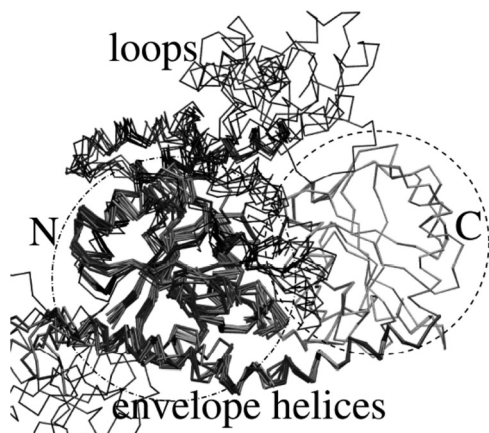


**Fig. 2.** Internal variation among the 10 lowest-energy UGT1A1 models of alignment c. In the C-terminal domain (thin lines at bottom) the models superimpose perfectly, reflecting high similarity between the template and target. The structurally conserved parts of the N-terminal domain (gray thick lines on the top) and the envelope helices, on the left, agree reasonably well among the models, but the variation is much more pronounced for loops 3 and 5 (thin black lines on the right).

within the N-terminal domain. In UGT1A3–UGT1A5 the residues to be glycosylated are Asn119 and Asn142 (UGT1A3 numbering), both of which are in loop 3. These residues correspond to Lys118 and Ala141 in UGT1A1, which are located in helix  $N\alpha 3$  and right after it. Both are on the surface of the protein and could be decorated with sugars. It is noteworthy that Asn189 of UGT1A3 in loop 5, corresponding to Asn188 of UGT1A1, is predicted *not* to be glycosylated because it is followed by a proline. Compared with the positively predicted sites, Asn189 is found on the opposite side of the globular domain, suggesting a possible lumen-membrane orientation for the protein. UGT1A7–UGT1A10 exhibit one strongly predicted glycosylation site at Asn71 (corresponding to Phe73 of UGT1A1), in the loop right before  $N\beta 3$ . UGT2A1 contains a strongly predicted glycosylation site at Asn49 before the start of  $N\beta 2$  (corresponding to Glu56 of UGT1A1). It is noteworthy that the three predicted sites in three different UGTs (UGT1A3: Asn142; UGT1A7: Asn71; UGT2A1: Asn49) all fall spatially quite close to each other in the model, even though they originate from different parts of the sequences. Taken together, the data suggest a spatially conserved glycosylation site before strands  $N\beta 2$ ,  $N\beta 3$ , or  $N\beta 4$ . We modeled an N-linked complex sugar to the loop between  $N\alpha 2$  and  $N\beta 3$  of UGT1A1.

**Bilirubin Binding.** With several protein–substrate complexes of GT-Bs available, the localization of the active site at the N/C-domain interface is unproblematic. The UDP-sugar analogs found in six GT-B proteins studied overlap very well; the maximal difference in the positions of the phosphates between any two structures is 1.2 Å (data not shown). The same position is expected to be valid for the UGTs, too.

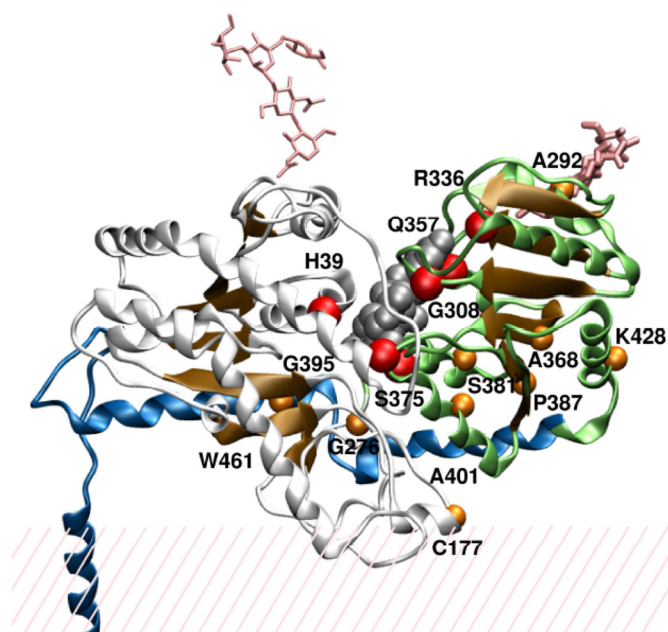


**Fig. 3.** Location of N-glycosylation sites and CN-I mutations in the UGT1A1 model. The N-terminal domain is shown in white, the C-terminal domain is shown in green, and the envelope helices and transmembrane helix are shown in blue. The gray space-filling molecule in the middle is the UDP-sugar. The pink stick structures represent the N-linked sugars. The one on the right is attached to Asn295 of UGT1A1, and the one on the left, shown by thin lines, shows the position where many other UGTs are predicted to be glycosylated. Red spheres highlight CN-I mutations that are located within 5 Å from the UDP-sugar, and the orange spheres sites are further from it.



Hence, a UDP-glucose analog was copied from one template, structure 2vce, to the UGT1A1 model. Bilirubin is highly flexible, but is known to exist in two internally hydrogen-bonded configurations in aqueous solutions: (Z,Z)-bilirubin and (Z,E)-bilirubin (Nogales and Lightner, 1995). Docking either of the free carbonyls in bilirubin between the active-site histidine and the anomeric carbon of the UDP-glucose places the rest of the molecule between loops 3 and 5. Not only His39 but the whole helix N $\alpha$ 1 lies quite close to the UDP-sugar and forms an active site wall. Asp36, Ser38, and Leu41 of N $\alpha$ 1 come within van der Waals distance from the UDP-sugar as does His376 of C $\alpha$ 4. There seems to be two alternative orientations for bilirubin binding, either toward loop 5 and the membrane or toward loop 3 and the endoplasmic reticulum lumen (Fig. 4). In the former orientation, bilirubin is in contact with residues Gln84, Asp87, Lys115, and Ile116, whereas in the latter it is in contact with Lys115, Ile116, Ala174, Val193, and Asp224. The contact sites are highly tentative, because loops 3 and 5 are largely nonhomologous to the templates. It should be mentioned, however, that the substrates in the known glycosyltransferase structures are found closer to loop 5 (data not shown).

**Comparison to Earlier Work.** One way to evaluate the current molecular model is to compare it with the earlier ones by Locuson and Tracy (2007) and Li and Wu (2007). They were published so close in time that no previous comparison exists. We have matched the template-target alignments from those studies to our own alignment and exam-

ined the results. The combination alignment is shown in Supplemental Fig. 2, and the differences in the positions of the secondary structure elements are listed in Table 2. Even without the UGT2B7 structure as a template, the models agree perfectly with each other between residues Gln288 and Arg467. The two earlier models do not continue past the C-terminal domain into the envelope helices and the transmembrane helix. In the N-terminal domain, N $\alpha$ 1–N $\beta$ 1 and N $\beta$ 4–N $\alpha$ 4–N $\beta$ 5 at the center of the domain are aligned identically to the template in the three models. For N $\beta$ 7 two models agree fully, whereas the third differs by a single residue. Our model resembles more closely that by Locuson and Tracy (2007). The average unsigned difference between the two models is 1.5 amino acids for the core domain. We were surprised to find that Locuson and Tracy had not aligned the structurally conserved N $\alpha$ 2 with anything, even though they had assigned the helix in the template structure. In their model, this segment must be a random coil, or there is a mistake in their figure 1. The next largest difference between the two models is in helix N $\alpha$ 6, by one helical turn. The similarity between the models is acceptable, with the exception of N $\alpha$ 2, and differences of the same magnitude are probably caused by variations in construction and optimization schemes of the molecular models. The model by Li and Wu (2007) differs more from our model and that by Locuson and Tracy (2007). The average unsigned differences in the positions of the secondary structure elements in the core N-terminal domain are very similar for both comparisons, 2.4 and 2.8, respectively. The differences arise from N $\alpha$ 2–N $\beta$ 3 and N $\beta$ 6–N $\alpha$ 6, and for the short  $\beta$ -strands especially the variations are crucial. It remains to be seen which assignment is correct.

## Discussion

Our goal in modeling the human UGT1A1 was to provide a structural framework in which to analyze biological data and formulate new functional hypotheses that could be tested experimentally. The common understanding is that the N-terminal half of the UGTs is variable, whereas the C-terminal half is conserved. According to our analysis this is an oversimplification. The C-terminal half is better seen as composed of three structural domains (Fig. 1), the largest of which, the C-terminal  $\alpha/\beta/\alpha$  sandwich, contains the UDP-GlcUA binding site. As for the degree of conservation, the hydrophobic core of the N-terminal  $\alpha/\beta/\alpha$  domain is equally well conserved as the core of the C-terminal domain. The variability of the N-terminal domain only holds for certain loop segments.

The differences between closely homologous human UGTs are found mainly in loop 3, in a segment called hypervariable region II (Ala61 to Tyr74) by Li and Wu (2007) in their

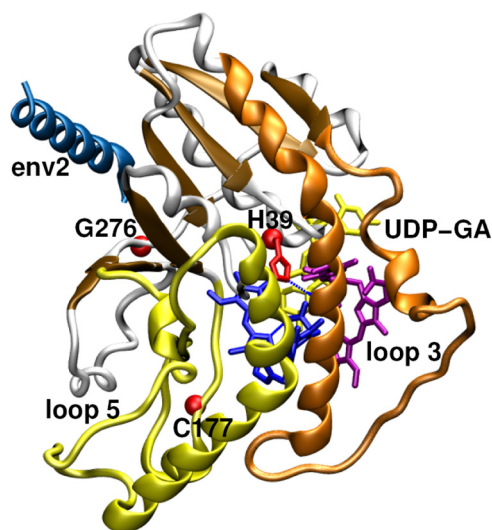


**Fig. 4.** Bilirubin in the active site of the UGT1A1. The image is viewed from the top of the N-terminal domain, and the second envelope helix is shown in blue on the left for orientation. Loop 3 is colored orange, and loop 5 is yellow. Histidine 39 is depicted as a red molecular structure in the middle of the protein. Two identical copies of bilirubin in Z,Z conformation are shown, oriented either more toward loop 3 or loop 5. The CN-I mutation sites in the N-terminal domain are marked by red spheres.

TABLE 2

Difference in the positions of the secondary structure elements in the N-terminal domain in three homology models of the human UGT1A1. The averages are calculated from unsigned differences; "average" values are those calculated without helix N $\alpha$ 3.

Source	N $\beta$ 1	N $\alpha$ 1	N $\beta$ 2	N $\alpha$ 2	N $\beta$ 3	N $\alpha$ 3	N $\beta$ 4	N $\alpha$ 4	N $\beta$ 5	N $\beta$ 6	N $\alpha$ 6	N $\beta$ 7	Average/"Average"
Li and Wu, 2007; current study	0	0	-2	-4	-5	+19	0	0	0	+8	+7	0	3.75/2.36
Locuson and Tracy, 2007; current study	0	0	-2	-9	0	+4	0	0	0	-1	-4	-1	1.75/1.54
Li and Wu, 2007/Locuson and Tracy, 2007	0	0	0	+5	+5	+15	0	0	0	+9	+11	+1	3.83/2.82

extensive sequence analysis. Modeling this region is uncertain, but needed for understanding substrate binding. Helix N $\alpha$ 3-3 packs to two helices of quite different character: the structurally well conserved N $\alpha$ 4 and the poorly defined N $\alpha$ 5-2 that corresponds to the hypervariable region IV (Ile215 to Pro229) of Li and Wu (2007). In the template structures, several interhelical contacts are seen within this helix triplet that seem to stabilize a second helical layer above the core  $\alpha/\beta$  structure. This may allow for more coherent movements of the variable part of loop 3 that seems to form one wall of the substrate binding pocket. Small substrates would bind between His39 and UDP-sugar without reaching out to contact loops 3 and 5, whereas larger ones such as bilirubin would touch the loops. Helix N $\alpha$ 3-1 would isolate the reaction site from bulk water and move concertedly to allow exit of the products.

The model drew our attention to two potentially interesting residues in loop 5, Cys177 and His173. Cys177 is conserved among UGT1As, and its replacement by arginine or tyrosine causes CN-I syndrome (Seppen et al., 1994; Ghosh et al., 2005). There is another conserved cysteine (Cys186) close by, but a previous study presented evidence against disulfide bonds in UGT1A1 (Ghosh et al., 2005). Neither are disulfides predicted for this segment by sequence analysis (Ceroni et al., 2006). Could Cys177 be palmitoylated and serve as an additional membrane attachment point within the N-terminal domain? Ciotti et al. (1998) predicted a membrane-embedded helix in UGT1A1 between cysteines 156 and 177. In our model, these residues fold into N $\alpha$ 4 and N $\beta$ 5 and continue for five residues into loop 5. A membrane attachment site after N $\beta$ 5 would agree with all three molecular models of UGT1A1. Another clue to membrane orientation is provided by the predicted N-linked glycosylation sites. There are two commonly glycosylated segments in the UGTs, one in C $\alpha$ 0 and another in the short loops between N $\beta$ 2 and N $\beta$ 4. When the molecule is oriented so that the putative glycosylation sites are fully solvated, some part of loop 5 probably contacts the membrane (Fig. 3). This proposal agrees with palmitoylated Cys177 forming the actual membrane contact. Nevertheless, because the corresponding residue in the UGTs of subfamilies 2A and 2B is either Ala or Gly, the possible acylation of Cys177 in UGT1As may not be essential for the membrane attachment of the enzymes.

His173 is located right at the beginning of loop 5, where the peptide chain runs past the bound UDP-sugar. His173 sits next

to the glucuronic acid and could form a hydrogen bond with its carboxylic group. In most human UGTs the locus is occupied by an arginine. Recently, a serine at the corresponding site was shown to correlate with glucuronic acid specificity in the plant UGT88D, whereas the main determinant for sugar selectivity in that case was Arg350 (Noguchi et al., 2009). Other residues suggested to bind to the carboxylic group are Arg53 and Arg254 (Radomska-Pandya et al., 2009).

The catalytic residues of the UGTs, a histidine at the beginning of N $\alpha$ 1 and an aspartate at the end of N $\beta$ 4, have been addressed in several studies (Li et al., 2007; Patana et al., 2008; Kerdpin et al., 2009). In UGT1A1, either Asp146 or Asp151 could be the critical acid. Data for corresponding aspartates in UGT1A6 (Li et al., 2007) and UGT1A9 (Patana et al., 2008) are conflicting. In UGT1A6, the Asp-to-Ala mutation abolished activity only at the latter position, whereas in UGT1A9 both mutants retain weak activity. The  $K_m$  increase for several substrates was larger for the latter position. We have constructed two alternative structures for the N $\beta$ 4 area. In the first structure, the aspartates are situated at the beginning and end of the sheet, and in the second, they are situated at the end of the sheet and in the following loop. The importance of the pre-N $\beta$ 4 position (Asp146), faraway from the active site, may be explained by interactions with N $\beta$ 1 and env2, whereas the post-N $\beta$ 4 acid (Asp151) polarizes the catalytic histidine.

The UGT database lists 15 different point mutations that lead to a full-length UGT1A1 that is functionally inactive, causing CN-I syndrome. These 15 amino acids were localized in the new UGT1A1 model (Fig. 3), and the surrounding structure was analyzed for possible reasons for the functional failure (Table 3 and Fig. 3). Only three CN-I mutations fall within the N-terminal domain: H39D, C177R, and G276R. Histidine 39 is situated in the structurally well conserved first helix of the protein and plays a major role in the catalytic reaction (Miley et al., 2007; Patana et al., 2008). The C177R mutation falls in the most variable segment of the protein, loop 5. G276R occurs at the beginning of the interdomain linker. Strikingly, Gly276 is fully conserved in most known GT-B structures.

The majority (12 of 15) of the pathological CN-I sites are found in the C-terminal domain. Five of them, G308E, R336W/Q/L, Q357R, S375R, and G395V lie within 5 Å of the UDP-sugar and can be considered as active-site mutations, together with H39D. Three additional ones (A368I, S381R, and P387R/S)

TABLE 3  
CN-I point mutations, their localization in the model, and hypothetical function  
Bold residues belong to the signature sequence.

Mutation	Localization in the Model	Suggested Function
H39D	First turn of N $\alpha$ 1	Catalytic residue
C177R	Early in loop 5	Possible palmitoylation site
G276R	In the linker, next to env1 and env2	Conserved Gly site
A292V	In C $\alpha$ 0, facing the solvent	Inhibits glycosylation at Asn295?
G308E	Right after C $\beta$ 1, packing to UDP	Disturbs the binding pocket
R336W/Q/L	Late in C $\beta$ 2, next to UDP	Interferes with the active site
<b>Q357R</b>	Starts C $\alpha$ 3, binds to uridine	Disturbs the binding pocket
<b>A368I</b>	Middle of C $\beta$ 4, packs to C $\alpha$ 6 and C $\beta$ 1	Interferes with packing
<b>S375R</b>	Starts C $\alpha$ 4, at domain interface	Interferes with packing
<b>S381R</b>	In C $\alpha$ 4, packed to C $\beta$ 4 and C $\beta$ 5	Conserved small residue site
<b>P387R/S</b>	Starts C $\beta$ 5, next to C $\alpha$ 6 and env1	Conserved Pro site
<b>G395V</b>	Before C $\alpha$ 5, next to UDP	Disturbs the binding pocket
A401P	In C $\alpha$ 5, packs tight to C $\beta$ 5 and C $\beta$ 6	Interferes with packing
K428E	In C $\alpha$ 6, contacts E424 and N425	Destabilizes domain interface
W461R	In env2, next to C $\beta$ 7	Interferes with packing



occur in the UGT signature sequence, Trp354 to Gln397. These residues are well conserved throughout all glycosyltransferases and participate in forming the hydrophobic core of the C domain. The remaining four CN-I mutations are A292V, A401P, K428E, and W461R. Ala292 is located in helix C $\alpha$ 0, three residues from the predicted N-glycosylation site Asn295. One may thus wonder whether a valine at this position could interfere somehow with the N-glycosylation of Asn295. We propose that mutations of Ala401, situated in the middle of C $\alpha$ 5, and Trp461, early in the second envelope helix, disrupt the hydrophobic packing of the protein. The last CN-I site, Lys428, is situated on the outer surface of the last helix, C $\alpha$ 6. In the model Lys428 forms salt bridges to Glu424 and Asn425 in the same helix and stabilizes the structure at the domain interphase. The 428E disease mutation could be linked to the interdomain motion.

Evaluating the functional importance of the CN-II or Gilbert syndrome sites is harder, specifically because their genetic background and possible related promoter mutations have not always been studied. Nevertheless, it may be interesting to note that the UGT database lists one Gilbert syndrome mutation in loop 3 (F83L) and one in loop 5 (P229Q). Three CN-II sites in loop 5 (L175Q, Q185P, and R209W) are also present.

In summary, we have modeled the full-length human UGT1A1 and gained new insights to central functional questions. The added features in the present model, the two structurally conserved envelope helices and the N-linked glycosyl groups, focus the analysis to the extensive interdomain contact surfaces and the probing of the luminal-membrane orientation.

## Acknowledgments

We thank Dr. J. Ravantti for advice and generous computer resources.

## References

- Altschul SF, Madden TL, Schäffer AA, Zhang J, Zhang Z, Miller W, and Lipman DJ (1997) Gapped BLAST and PSI-BLAST: a new generation of protein database search programs. *Nucleic Acids Res* **25**:3389–3402.
- Barton GJ (1993) ALSCRIPT: a tool to format multiple sequence alignments. *Protein Eng* **6**:37–40.
- Berman HM, Westbrook J, Feng Z, Gilliland G, Bhat TN, Weissig H, Shindyalov IN, and Bourne PE (2000) The Protein Data Bank. *Nucleic Acids Res* **28**:235–242.
- Bosma PJ, Seppen J, Goldhoorn B, Bakker C, Oude Elferink RP, Chowdhury JR, Chowdhury NR, and Jansen PL (1994) Bilirubin UDP-glucuronosyltransferase 1 is the only relevant bilirubin glucuronidating isoform in man. *J Biol Chem* **269**:17960–17964.
- Brazier-Hicks M, Offen WA, Gershtater MC, Revett TJ, Lim EK, Bowles DJ, Davies GJ, and Edwards R (2007) Characterization and engineering of the bifunctional N- and O-glucosyltransferase involved in xenobiotic metabolism in plants. *Proc Natl Acad Sci USA* **104**:20238–20243.
- Ceroni A, Passerini A, Vullo A, and Frasconi P (2006) DISULFIND: a disulfide bonding state and cysteine connectivity prediction server. *Nucleic Acids Res* **34**:W177–W181.
- Ciotti M, Cho JW, George J, and Owens IS (1998) Required buried  $\alpha$ -helical structure in the bilirubin UDP-glucuronosyltransferase UGT1A1 contains a nonreplaceable phenylalanine. *Biochemistry* **37**:11018–11025.
- Davis IW, Leaver-Fay A, Chen VB, Block JN, Kapral GJ, Wang X, Murray LW, Arendall WB 3rd, Snoeyink J, Richardson JS, et al. (2007) MolProbity: all-atom contacts and structure validation for proteins and nucleic acids. *Nucleic Acids Res* **35**:W375–W383.
- Finel M and Kurkela M (2008) The UDP-glucuronosyltransferases as oligomeric enzymes. *Curr Drug Metab* **9**:70–76.
- Fujiwara R, Nakajima M, Yamamoto T, Nagao H, and Yokoi T (2009a) In silico and in vitro approaches to elucidate the thermal stability of human UDP-glucuronosyltransferase (UGT) 1A9. *Drug Metab Pharmacokinet* **24**:235–244.
- Fujiwara R, Nakajima M, Yamanaka H, and Yokoi T (2009b) Key amino acid residues responsible for the differences in substrate specificity of human UDP-glucuronosyltransferase (UGT)1A9 and UGT1A8. *Drug Metab Dispos* **37**:41–46.
- Ghosh SS, Lu Y, Lee SW, Wang X, Guha C, Roy-Chowdhury J, and Roy-Chowdhury N (2005) Role of cysteine residues in the function of human UDP glucuronosyltransferase isoform 1A1 (UGT1A1). *Biochem J* **392**:685–692.
- Hans J, Brandt W, and Vogt T (2004) Site-directed mutagenesis and protein 3D-homology modelling suggest a catalytic mechanism for UDP-glucose-dependent betanidin 5-O-glucosyltransferase from *Dorotheanthus bellidiformis*. *Plant J* **39**:319–333.
- Holm L, Kääriäinen S, Rosenström P, and Schenkel A (2008) Searching protein structure databases with DALI Lite v.3. *Bioinformatics* **24**:2780–2781.
- Humphrey W, Dalke A, and Schulten K (1996) VMD: visual molecular dynamics. *J Mol Graph* **14**:27–28, 33–38.
- Kerdpin O, Mackenzie PI, Bowalgha K, Finel M, and Miners JO (2009) Influence of N-terminal domain histidine and proline residues on the substrate selectivities of human UDP-glucuronosyltransferase 1A1, 1A6, 1A9, 2B7, and 2B10. *Drug Metab Dispos* **37**:1948–1955.
- Kurkela M, Hirvonen J, Kostiainen R, and Finel M (2004a) The interactions between the N-terminal and C-terminal domains of the human UDP-glucuronosyltransferases are partly isoform-specific, and may involve both monomers. *Biochem Pharmacol* **68**:2443–2450.
- Kurkela M, Mörsky S, Hirvonen J, Kostiainen R, and Finel M (2004b) An active and water-soluble truncation mutant of the human UDP-glucuronosyltransferase 1A9. *Mol Pharmacol* **65**:826–831.
- Lairson LL, Henrissat B, Davies GJ, and Withers SG (2008) Glycosyltransferases: structures, functions, and mechanisms. *Annu Rev Biochem* **77**:521–555.
- Larkin MA, Blackshields G, Brown NP, Chenna R, McGettigan PA, McWilliam H, Valentin F, Wallace IM, Wilm A, Lopez R, et al. (2007) Clustal W and Clustal X version 2.0. *Bioinformatics* **23**:2947–2948.
- Lewis BC, Mackenzie PI, Elliot DJ, Burchell B, Bhasker CR, and Miners JO (2007) Amino terminal domains of human UDP-glucuronosyltransferases (UGT) 2B7 and 2B15 associated with substrate selectivity and autoactivation. *Biochem Pharmacol* **73**:1463–1473.
- Li C and Wu Q (2007) Adaptive evolution of multiple-variable exons and structural diversity of drug-metabolizing enzymes. *BMC Evol Biol* **7**:69.
- Li D, Fournel-Gigleux S, Barré L, Mulliert G, Netter P, Magdalou J, and Ouzzine M (2007) Identification of aspartic acid and histidine residues mediating the reaction mechanism and the substrate specificity of the human UDP-glucuronosyltransferases 1A. *J Biol Chem* **282**:36514–36524.
- Locuson CW and Tracy TS (2007) Comparative modelling of the human UDP-glucuronosyltransferases: insights into structure and mechanism. *Xenobiotica* **37**:155–168.
- Luukkainen L, Taskinen J, Kurkela M, Kostiainen R, Hirvonen J, and Finel M (2005) Kinetic characterization of the 1A subfamily of recombinant human UDP-glucuronosyltransferases. *Drug Metab Dispos* **33**:1017–1026.
- Mackenzie PI, Bock KW, Burchell B, Guillemette C, Ikushiro S, Iyanagi T, Miners JO, Owens IS, and Nebert DW (2005) Nomenclature update for the mammalian UDP glucosyltransferase (UGT) gene superfamily. *Pharmacogenet Genomics* **15**:677–685.
- Meech R, Yogalingam G, and Mackenzie PI (1996) Mutational analysis of the carboxy-terminal region of UDP-glucuronosyltransferase 2B1. *DNA Cell Biol* **15**:489–494.
- Miley MJ, Zielinska AK, Keenan JE, Bratton SM, Radomska-Pandya A, and Redinbo MR (2007) Crystal structure of the cofactor-binding domain of the human phase II drug-metabolism enzyme UDP-glucuronosyltransferase 2B7. *J Mol Biol* **369**:498–511.
- Nishiyama T, Fujishima M, Masuda Y, Izawa T, Ohnuma T, Ogura K, and Hiratsuka A (2008) Amino acid positions 69–132 of UGT1A9 are involved in the C-glucuronidation of phenylbutazone. *Arch Biochem Biophys* **478**:75–80.
- Nogales D and Lightner DA (1995) On the structure of bilirubin in solution. <sup>13</sup>C[1H] heteronuclear Overhauser effect NMR analyses in aqueous buffer and organic solvents. *J Biol Chem* **270**:73–77.
- Noguchi A, Horikawa M, Fukui Y, Fukuchi-Mizutani M, Iuchi-Okada A, Ishiguro M, Kiso Y, Nakayama T, and Ono E (2009) Local differentiation of sugar donor specificity of flavonoid glycosyltransferase in Lamiales. *Plant Cell* **21**:1556–1572.
- Osmani SA, Bak S, Imberty A, Olsen CE, and Möller BL (2008) Catalytic key amino acids and UDP-sugar donor specificity of a plant glucuronosyltransferase, UGT94B1: molecular modeling substantiated by site-specific mutagenesis and biochemical analyses. *Plant Physiol* **148**:1295–1308.
- Ouzzine M, Magdalou J, Burchell B, and Fournel-Gigleux S (1999) An internal signal sequence mediates the targeting and retention of the human UDP-glucuronosyltransferase 1A6 to the endoplasmic reticulum. *J Biol Chem* **274**:31401–31409.
- Patana AS, Kurkela M, Finel M, and Goldman A (2008) Mutation analysis in UGT1A9 suggests a relationship between substrate and catalytic residues in UDP-glucuronosyltransferases. *Protein Eng Des Sel* **21**:537–543.
- Radomska-Pandya A, Bratton SM, Redinbo MR, and Miley MJ (2010) The crystal structure of human UDP-glucuronosyltransferase 2B7 C-terminal end is the first mammalian UGT target to be revealed: the significance for human UGTs from both the 1A and 2B families. *Drug Metab Rev* **42**:128–139.
- Rost B, Yachdav G, and Liu J (2004) The PredictProtein server. *Nucleic Acids Res* **32**:W321–W326.
- Sali A and Blundell TL (1993) Comparative protein modelling by satisfaction of spatial restraints. *J Mol Biol* **234**:779–815.
- Seppen J, Bosma PJ, Goldhoorn BG, Bakker CT, Chowdhury JR, Chowdhury NR, Jansen PL, and Oude Elferink RP (1994) Discrimination between Crigler-Najjar type I and II by expression of mutant bilirubin uridine diphosphate-glucuronosyltransferase. *J Clin Invest* **94**:2385–2391.
- Stewart JJ (2007) Optimization of parameters for semiempirical methods V: modification of NDDO approximations and application to 70 elements. *J Mol Model* **13**:1173–1213.
- Thorsøe KS, Bak S, Olsen CE, Imberty A, Breton C, and Lindberg Möller B (2005) Determination of catalytic key amino acids and UDP sugar donor specificity of the cyanohydrin glycosyltransferase UGT85B1 from *Sorghum bicolor*. Molecular modeling substantiated by site-specific mutagenesis and biochemical analyses. *Plant Physiol* **139**:664–673.
- Unligil UM and Rini JM (2000) Glycosyltransferase structure and mechanism. *Curr Opin Struct Biol* **10**:510–517.
- White SH (2009) Biophysical dissection of membrane proteins. *Nature* **459**:344–346.

**Address correspondence to:** Moshe Finel, University of Helsinki, P.O. Box 56 (Viikinkaari 5), 00014, Helsinki, Finland. E-mail: moshe.finel@helsinki.fi